ICI Mitigation for Pilot-Aided OFDM Mobile Systems

Yasamin Mostofi, *Member, IEEE* and Donald C. Cox, *Fellow, IEEE*

Abstract—Orthogonal frequency-division multiplexing (OFDM) is robust against frequency selective fading due to the increase of the symbol duration. However, for mobile applications channel time-variations in one OFDM symbol introduce intercarrier-interference (ICI) which degrades the performance. This becomes more severe as mobile speed, carrier frequency or OFDM symbol duration increases. As delay spread increases, symbol duration should also increase in order to maintain a near-constant channel in every frequency subband. Also, due to the high demand for bandwidth, there is a trend toward higher carrier frequencies. Therefore, to have an acceptable reception quality for the applications that experience high delay and Doppler spread, there is a need for ICI mitigation within one OFDM symbol. We introduce two new methods to mitigate ICI in an OFDM system with coherent channel estimation. Both methods use a piece-wise linear model to approximate channel time-variations. The first method extracts channel time-variations information from the cyclic prefix. The second method estimates these variations using the next symbol. We find a closed-form expression for the improvement in average signal-to-interference ratio (SIR) when our mitigation methods are applied for a narrowband time-variant channel. Finally, our simulation results show how these methods would improve the performance in a highly time-variant environment with high delay spread.

Index Terms—Channel estimation, intercarrier-interference (ICI) mitigation, mobility, orthogonal frequency-division multiplexing (OFDM).

I. INTRODUCTION

ORTHOGONAL frequency-division multiplexing (OFDM) handles frequency selective fading resulting from delay spread by expanding the symbol duration [1]–[4]. By adding a guard interval to the beginning of each OFDM symbol, the effect of delay spread (provided that there is perfect synchronization) would appear as a multiplication in the frequency domain for a time-invariant channel.[1] This feature allows for higher data rates and has resulted in the selection of OFDM as a standard for digital audio broadcasting (DAB [5]), digital video broadcasting (DVB [6]), and wireless local area networks (802.11a).

Transmission in a mobile communication environment is impaired by both delay and Doppler spread. As delay spread increases, symbol duration should also increase for two reasons. First, most receivers require a near-constant channel in each frequency subband. As delay spread increases, this can be achieved by an increase of the symbol length. Second, to prevent inter-OFDM symbol-interference, the length of the guard interval should increase as well. Therefore, to reduce redundancy, the symbol length should increase [7]. OFDM systems become more susceptible to time-variations as symbol length increases. Time-variations introduce ICI, which must be mitigated to improve the performance in high delay and Doppler spread environments.

In [8] and [9], authors analyzed the effect of ICI by modeling it as Gaussian noise. A simplified bound on ICI power has also been derived [10]. To mitigate the introduced ICI, techniques using receiver antenna diversity have been proposed [8], [11]. However, sensitivity analysis has shown that as normalized Doppler spread (defined as the maximum Doppler spread divided by the sub-carrier spacing) increases, antenna diversity becomes less effective in mitigating ICI in OFDM mobile systems [12].

Jeon and Chang have proposed another method for ICI mitigation which assumes a linear model for channel variations [13]. However, they assumed that some of the coefficients of the channel matrix are negligible, which is only the case under low Doppler and delay spread conditions. For instance, their results showed performance improvement under normalized Doppler of up to 2.72% and delay spread of 2 μs for a two-tap channel. In high-mobility applications that require ICI mitigation, however, delay spread can be much longer. For instance, the delay spread can be as high as 40 μs for single frequency network (SFN) channels[2] and 20 μs for cellular applications. Furthermore, normalized Doppler can get as high as 10% depending on the carrier frequency. Their method also relies on the information of adjacent OFDM symbols for channel estimation, which increases processing delay.

To improve the performance in high delay and Doppler spread environments, we present two new ICI mitigation methods in this paper. Unlike the method of Jeon *et al.*, our methods can mitigate ICI in considerably high delay and Doppler spread applications such as SFN and cellular networks. Furthermore, in Method I, we mitigate ICI without relying on the adjacent symbols. Both of our methods are based on a piece-wise linear approximation for channel time-variations.

[1]Adding the guard interval will also prevent inter-OFDM symbol-interference.

[2]SFN refers to DAB and DVB type environments in which adjacent base stations transmit in the same frequencies to save the bandwidth.

In the absence of time-variations, frequency domain pilot tones or differential modulation should be used to remove the effect of channel frequency-variations. As the delay spread increases, differential modulation across adjacent subbands degrades the performance. As mobility and/or the length of the OFDM symbol increase, differential modulation across adjacent symbols leads to performance loss as well. Therefore, we use frequency domain pilot tones in this paper since we are dealing with high delay and Doppler spread environments. The minimum number of pilot tones required in each symbol exceeds normalized channel delay spread[3] by one [14]. These pilot tones should be equally spaced in the frequency domain to minimize noise enhancement [14].

In the presence of Doppler spread, however, these pilot tones can not estimate channel time-variations. In this work, we show how to estimate these variations utilizing either the cyclic prefix or the next symbol. Finally, our analysis and simulation results show performance improvement in high delay and Doppler spread environments.

II. SYSTEM MODEL

Fig. 1 shows the discrete baseband equivalent system model. We assume perfect timing synchronization in this paper. More information on timing synchronization for a pilot-aided OFDM system can be found in [15]. The available bandwidth is divided into N subchannels and the guard interval spans G sampling periods. We assume that the normalized length of the channel is always less than or equal to G in this paper. X_i represents the transmitted data point in the ith frequency subband and is related to the time domain sequence, x, as follows:

$$X_i = \sum_{k=0}^{N-1} x_k e^{-\frac{j2\pi ki}{N}} \quad 0 \le i \le N-1. \tag{1}$$

$\vec{x}_p$ is the cyclic prefix vector with length G and is related to x as follows:

$$\vec{x}_p(i) = x_{N-G+i} \quad 0 \le i \le G-1. \tag{2}$$

Let T be the time duration of one OFDM symbol after adding the guard interval. Then, $h_k^{(i)}$ represents the kth channel tap at time instant $t = i \times T_s$ where $T_s = T/(N+G)$ is the sampling period. A constant channel is assumed over the time interval $i \times T_s \le t < (i+1) \times T_s$ with $t = 0$ indicating the start of the data part of the symbol. $h_k^{(i)}$ for $-G \le i \le -1$ and $0 \le i \le N-1$ represents the kth channel tap in the guard and data interval respectively.

The channel output y can then be expressed as follows:

$$y_i = \sum_{k=0}^{G} h_k^{(i)} x_{((i-k))_N} + w_i \quad 0 \le i \le N-1. \tag{3}$$

In (3), $((\quad))_N$ represents a cyclic shift in the base of N and w_i represents a sample of additive white Gaussian noise. Then,
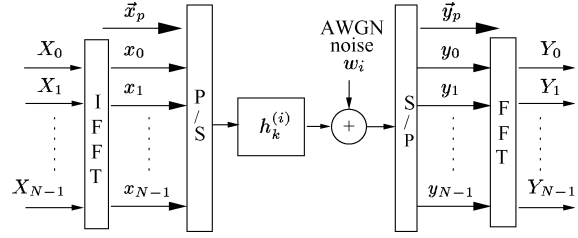
Fig. 1.   Discrete baseband equivalent system model.

Y, the fast Fourier transform (FFT) of sequence y, will be as follows:

$$Y_i = H_{i,0} X_i + \underbrace{\sum_{d=1}^{N-1} H_{i,d} X_{((i-d))_N}}_{ICI} + W_i \quad 0 \le i \le N-1 \tag{4}$$

where W denotes the FFT of w and the second term on the right hand side of (4) represents ICI. Define F_m as the FFT of the mth channel tap with respect to time-variations:

$$F_m(k) = \sum_{u=0}^{N-1} h_m^{(u)} e^{-\frac{j2\pi uk}{N}} \quad 0 \le m \le G \quad \& \quad 0 \le k \le N-1. \tag{5}$$

Then $H_{i,d}$ can be defined as

$$H_{i,d} = \frac{1}{N} \sum_{m=0}^{G} F_m(d) e^{-\frac{j2\pi m(i-d)}{N}} \quad 0 \le i, d \le N-1. \tag{6}$$

Furthermore, $H_{i,0} = \sum_{m=0}^{G} h_m^{\text{ave}} e^{\frac{-j2\pi mi}{N}}$ where $h_m^{\text{ave}} = (1/N)\sum_{u=0}^{N-1} h_m^{(u)}$ is the average of the mth channel tap over the time duration of $0 \le t < N \times T_s$. Therefore, $H_{i,0}$ represents the FFT of this average (note that h_m^{ave} solely refers to a time averaging over symbol data part and is different from channel ensemble average).

As was noted by previous work, the ICI term on the right-hand side of (4) can not be neglected as the maximum Doppler shift, f_d, increases (e.g., [8]).

III. PILOT EXTRACTION

Let $\nu \le G$ be the maximum predicted normalized length of the channel. In this paper, we assume that the normalized length of the channel is always smaller than ν. We insert $L \ge \nu + 1$ equally spaced pilots, P_{l_i}, at subchannels $l_i = (i \times N)/L$ for $0 \le i \le L-1$. An estimate of $H_{i,0}$ can then be acquired at pilot tones as follows:

$$\hat{H}_{l_i,0} = \frac{Y_{l_i}}{P_{l_i}} = H_{l_i,0} + \frac{(I_{l_i} + W_{l_i})}{P_{l_i}} \quad 0 \le i \le L-1. \tag{7}$$

In (7), I_{l_i} denotes ICI [marked in (4)] at l_ith subcarrier. Through an IFFT of length L, the estimate of h_k^{ave} would be

$$\hat{h}_k^{\text{ave}} = \frac{1}{L} \sum_{i=0}^{L-1} \hat{H}_{l_i,0} e^{\frac{j2\pi ik}{L}} \quad 0 \le k \le L-1. \tag{8}$$
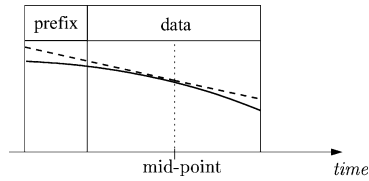
Fig. 2. Piece-wise linear model in one received OFDM symbol. Solid curve: real or imaginary part of a channel path. Dashed line: piece-wise linear model.

In the absence of mobility, L pilots would have been enough to estimate the channel. However in the presence of Doppler, due to the ICI term of (4), using the estimate of $\hat{h}_k^{\text{ave}}$ for data detection results in poor performance. This motivates the need to mitigate the resultant ICI.

IV. PIECE-WISE LINEAR APPROXIMATION

In this paper, we approximate channel time-variations with a piece-wise linear model with a constant slope over the time duration T (Fig. 2). For normalized Doppler of up to 20%, linear approximation is a good estimate of channel time-variations and the effect on correlation characteristics is negligible. To see this, Appendix A shows how this approximation affects the correlation function as normalized Doppler increases.

In this section, we will derive the frequency domain relationship, similar to (4), when the linear approximation is applied. Let α_k denote the slope of the kth channel tap in the current OFDM symbol. To perform the linearization, knowledge of the channel at one time instant in the symbol is necessary. Let $E(z)$ represent the average of z. Then for the kth channel tap, $E(|h_k^{\text{ave}} - h_k^{(s)}|^2)$ is minimized for $s = \left(\frac{N}{2} - 1\right)$ as is shown in Appendix B. Therefore, we approximate $h_k^{\left(\frac{N}{2}-1\right)}$ with the estimate of h_k^{ave}. We will have

$$\hat{h}_k^{\left(\frac{N}{2}-1\right)} = \hat{h}_k^{\text{ave}}. \tag{9}$$

Consider linearization around $h_k^{\left(\frac{N}{2}-1\right)}$. Then, $h_k^{(i)}$ can be approximated as follows:

$$h_k^{(i)} \approx h_k^{\left(\frac{N}{2}-1\right)} + \left(i + 1 - \frac{N}{2}\right) \times \alpha_k \times T_s \quad 0 \le i \le N-1. \tag{10}$$

Inserting (10) into (3), we will have

$$\vec{y} \approx (\mathbf{h}_{\text{mid}} + \mathbf{M} \times \mathbf{A}) \times \vec{x} + \vec{w} \tag{11}$$

where $\vec{y}$, $\vec{x}$, and $\vec{w}$ are $N \times 1$ vectors containing samples of y_i, x_i, and w_i for $0 \le i \le N-1$. Furthermore, for $1 \le k, m \le N$, we will have

$$\mathbf{h}_{\text{mid}}(k, m)$$
$$= \begin{cases} h_{((k-m))_N}^{\left(\frac{N}{2}-1\right)} & 0 \le k - m \le G \quad \& \\ & -(N-1) \le k - m \le -(N-G) \\ 0 & else \end{cases} \tag{12}$$

$$\mathbf{A}(k, m)$$
$$= \begin{cases} \alpha_{((k-m))_N} & 0 \le k - m \le G \quad \& \\ & -(N-1) \le k - m \le -(N-G) \\ 0 & else. \end{cases} \tag{13}$$

$\mathbf{M}$ is a diagonal matrix with diagonal elements of $\mathbf{M}(k, k) = \beta_{k-1} = T_s \times (k - \frac{N}{2})$ for $1 \le k \le N$. It is shown in Appendix C that taking an FFT of $\vec{y}$ will result in the following frequency domain relationship:

$$\vec{Y} \approx \mathbf{H}_{\text{mid}}\vec{X} + \mathbf{C} \times \mathbf{H}_{\text{slope}}\vec{X} + \vec{W} \tag{14}$$

where

$$\mathbf{H}_{\text{mid}} = \text{diag}\left\{ FFT\left(\left[h_0^{\left(\frac{N}{2}-1\right)} \quad h_1^{\left(\frac{N}{2}-1\right)} \right. \right.\right.$$
$$\left.\left.\left. \cdots \quad h_G^{\left(\frac{N}{2}-1\right)} \quad 0 \quad \cdots \quad 0 \right] \right) \right\} \tag{15}$$

$$\mathbf{H}_{\text{slope}} = \text{diag}\left\{ FFT\left([\alpha_0 \quad \alpha_1 \quad \cdots \quad \alpha_G \quad 0 \quad \cdots \quad 0] \right) \right\}. \tag{16}$$

Here, $FFT(\vec{z})$ represents the FFT of the vector $\vec{z}$. $\vec{W}$ is a vector containing the FFT of noise samples and $\mathbf{C}_{n,m} = \frac{B_{n-m}}{N}$ where B is the FFT of β and is defined as follows:

$$B_k = T_s \times N \times \begin{cases} -\frac{1}{1 - e^{-\frac{j2\pi k}{N}}} & k \ne 0 \\ 0.5 & k = 0 \end{cases} \tag{17}$$

To solve (14) for $\vec{X}$, both $\mathbf{H}_{\text{mid}}$ and $\mathbf{H}_{\text{slope}}$ should be estimated. Matrix $\mathbf{C}$ is a fixed matrix that is precalculated and stored in the receiver. An estimate of $\mathbf{H}_{\text{mid}}$ is readily available from (7)–(9) and (15). In the following subsections, we show how to estimate $\mathbf{H}_{\text{slope}}$ with our two methods. In Method I, this is done by utilizing the redundancy of the cyclic prefix while in Method II the information of the next symbol is used.

A. Method I: ICI Mitigation Using Cyclic Prefix

The output prefix vector, $\vec{y}_p$ of Fig. 1, can be written as follows:

$$\vec{y}_p = \mathbf{Q} \times \vec{p} + \vec{w}_p. \tag{18}$$

In (18), $\vec{p} = \begin{bmatrix} \vec{x}_p^{pre} \\ \vec{x}_p \end{bmatrix}$, $\vec{w}_p$ contains AWGN samples and

$$\mathbf{Q}(i, j) = h_{((i-j+G))_{2 \times G}}^{(-G+i-1)} \quad 1 \le i \le G \quad 1 \le j \le 2 \times G. \tag{19}$$

Since $\nu \le G$, $h_k^{(i)} = 0$ for $k > G$ in matrix $\mathbf{Q}$. $\vec{x}_p$ is a $G \times 1$ vector defined in (2). $\vec{x}_p^{pre}$ is similarly defined for the transmitted cyclic prefix of the previous OFDM symbol and is already known to the receiver. Define $\vec{\zeta}$ as a vector containing slopes of all the taps

$$\vec{\zeta} = [\alpha_0 \quad \alpha_1 \quad \cdots \quad \alpha_G]^t. \tag{20}$$

Inserting $h_k^{(i)}$ from (10) in $\mathbf{Q}$, it can be easily shown that (18) can be written as follows:

$$\vec{y}_p - \mathbf{R} \times \vec{p} \approx \mathbf{D} \times \mathbf{X}_{p_{\text{mat}}} \times \vec{\zeta} + \vec{w}_p \tag{21}$$

Here, $\mathbf{R}(i, j) = h_{((i-j+G))_{2 \times G}}^{\left(\frac{N}{2}-1\right)}$ for $1 \le i \le G$ and $1 \le j \le 2 \times G$ and can be estimated from (7)–(9). $\mathbf{D}$ is a predetermined

TABLE I
PROCEDURE FOR METHOD I

Step	Command
1	Set the initial estimate of $\mathbf{H}_{slope}$ to zero
2	Use Eq. 7-9 & 15 to estimate $\mathbf{H}_{mid}$ from pilots
3	Solve Eq. 14 for $\vec{X}$
4	Solve Eq. 21 for $\vec{\zeta}$
5	Use Eq. 16 to estimate $\mathbf{H}_{slope}$
6	If not converged or timed out, go to step 3

diagonal matrix with $\mathbf{D}(i,i) = T_s \times (-\frac{N}{2} + i - G)$ for $1 \leq i \leq G$ and is stored in the receiver. $\mathbf{X}_{p_{mat}}$ is defined as follows:

$$\mathbf{X}_{p_{mat}} = \begin{bmatrix} Rev(\vec{p}^t[1:G+1]) \\ Rev(\vec{p}^t[2:G+2]) \\ \vdots \\ Rev(\vec{p}^t[G:2\times G]) \end{bmatrix} \quad (22)$$

where $Rev(\vec{J}[i:j])$ represents the vector produced by reversing the order of elements i through j of vector $\vec{J}$ and $\vec{J}^t$ denotes transpose of $\vec{J}$. Equations (14) and (21) provide enough information to solve for $\vec{X}$. There are two sets of unknowns, $\vec{X}$ and $\vec{\zeta}$ ($\mathbf{H}_{slope}$ is formed from FFT of $\vec{\zeta}$). It is possible to combine both equations to form a new one that is only a function of $\vec{X}$. However, the complexity of solving such an equation would be high. Therefore, we use a simpler iterative approach to solve for $\vec{X}$. We start with an initial estimate for $\vec{X}$ and $\vec{\zeta}$. In each iteration, we improve the estimate of $\vec{X}$ using (14) and then improve the estimate of $\vec{\zeta}$ using (21). This procedure is summarized in Table I.

B. Method II: ICI Mitigation Utilizing Adjacent Symbols

It is possible to acquire channel slopes without using the redundancy of the cyclic prefix. This can be done by utilizing either the previous symbol or both adjacent symbols. A constant slope is assumed over the time duration of $T + (N/2) \times T_s$ for the former and T for the latter. Therefore, the former can handle lower Doppler values while adding no processing delay. On the other hand, the latter would have a better performance at the price of delay of reception of the next symbol. Since we are interested in ICI mitigation in high mobility environments, we utilize both adjacent symbols to acquire channel slopes. This is shown in Fig. 3. Pilots of the current symbol provide an estimate of the channel at the mid-point of the current symbol, $\hat{h}_k^{(\frac{N}{2}-1)}$. This estimate is stored in the system. Upon processing of the next symbol, an estimate of the channel at midpoint of the next symbol, $\hat{h}_k^{(\frac{N}{2}-1),next}$, becomes available. Estimate of the slopes in region 2 (see Fig. 3) can then be obtained as follows:

$$\hat{\alpha}_k^{r_2} = \frac{\hat{h}_k^{(\frac{N}{2}-1),next} - \hat{h}_k^{(\frac{N}{2}-1)}}{T} \quad 0 \leq k \leq G \quad (23)$$
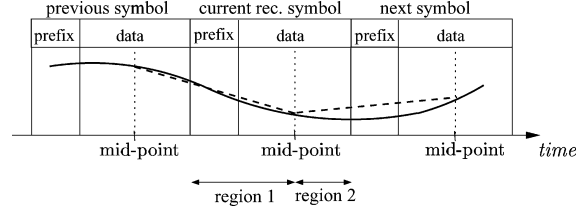

Fig. 3. Piece-wise linear model for method II. Solid curve: real or imag. part of a channel path. Dashed line: piece-wise linear model.

where $\alpha_k^{r_2}$ represents the slope of the kth channel tap in region 2. Similarly, $\alpha_k^{r_1}$, the slope in region 1, is estimated while processing the previous OFDM symbol and is stored in the receiver. Utilizing two slopes introduces a minor change in (11). It can be shown that in this case, we will have

$$\vec{y}_{method_{II}} \approx (\mathbf{h}_{mid} + \mathbf{M}^{r_1} \times \mathbf{A}^{r_1} + \mathbf{M}^{r_2} \times \mathbf{A}^{r_2}) \times \vec{x} + \vec{w}. \quad (24)$$

In (24), $\mathbf{A}^{r_m}$ represents channel slope matrix of (13) in the mth region ($1 \leq m \leq 2$) with $\mathbf{M}^{r_1}$ and $\mathbf{M}^{r_2}$ defined as follows:

$$\mathbf{M}^{r_1}(i,j) = \begin{cases} \mathbf{M}(i,j) & i = j \ \& \ 0 \leq i \leq \frac{N}{2} - 1 \\ 0 & else \end{cases}$$

$$\mathbf{M}^{r_2}(i,j) = \begin{cases} \mathbf{M}(i,j) & i = j \ \& \ \frac{N}{2} \leq i \leq N - 1. \\ 0 & else \end{cases} \quad (25)$$

Following the same procedure of Appendix C, it can be easily shown that the frequency domain relationship will be

$$\vec{Y}_{method_{II}} \approx \mathbf{H}_{mid}\vec{X} + \left(\mathbf{C}^{r_1} \times \mathbf{H}^{r_1}_{slope} + \mathbf{C}^{r_2} \times \mathbf{H}^{r_2}_{slope}\right) \times \vec{X} + \vec{W} \quad (26)$$

In (26), $\mathbf{H}^{r_m}_{slope}$ is the diagonal matrix defined in (16) for the slopes of the mth region and can be formed from $\hat{\alpha}_k^{r_m}$. $\mathbf{C}^{r_1}$ and $\mathbf{C}^{r_2}$ are fixed matrices. It can be easily shown that

$$\mathbf{C}^{r_1}(n,m)$$
$$= T_s \times \begin{cases} \frac{-.5}{1-e^{\frac{-j2\pi(n-m)}{N}}} + \frac{1-(-1)^{n-m}}{N \times \left(1-e^{\frac{-j2\pi(n-m)}{N}}\right)^2} & n \neq m \\ \frac{1}{4} - \frac{N}{8} & n = m \end{cases}$$

$$\mathbf{C}^{r_2}(n,m)$$
$$= T_s \times \begin{cases} \frac{-.5}{1-e^{\frac{-j2\pi(n-m)}{N}}} - \frac{1-(-1)^{n-m}}{N \times \left(1-e^{\frac{-j2\pi(n-m)}{N}}\right)^2} & n \neq m \\ \frac{1}{4} + \frac{N}{8} & n = m \end{cases} \quad (27)$$

An estimate of X can then be obtained from (26).

C. Complexity Analysis

In general, solving (14) and (21) in case of Method I and (26) or (24) in case of Method II requires matrix inversion which could increase receiver complexity. For Method I, since the size of (21) is smaller, the main complexity is in solving (14). This requires an $N \times N$ matrix inversion. In general, any matrix inversion algorithm can be used. Also, (14) and (26) show a special structure. For instance, in (14) we need to invert a sum of $diagonal + toeplitz \times diagonal$. The special structure can be used to reduce the complexity in iterative methods. Comparing

with the method proposed in [13], Methods I and II can handle considerably higher delay and Doppler spread (see Section I) at the price of higher computational complexity (by neglecting some of the channel coefficients, the complexity of the method proposed in [13] is reduced to $N - q$ inversions of a matrix of size $q \times q$, where q is smaller than N). However, depending on the computational power of the receiver, other less complex methods like conjugate gradient can be used for matrix inversion. A good survey of such methods and their complexity analysis can be found in [16], [17]. Furthermore, Section VI shows how adding a noise/interference reduction mechanism can further reduce the complexity.

Another important issue is the convergence property of Method I. In general, for the range of Doppler values that the piece-wise linear approximation can be applied, channel slopes are small enough that the initial estimate of zero in the first step of Method I results in the convergence of the method after a few iterations. A more detailed analysis of convergence properties of such iterative methods is beyond the scope of this paper but can be found in [17], [18].

V. MATHEMATICAL ANALYSIS OF THE EFFECT OF LINEARIZATION

In this section, we provide a mathematical analysis of the effect of piece-wise linear approximation in mitigating ICI. We assume a narrowband time-variant channel to make the analysis tractable and leave the case of wideband channels to our simulations in Section VII. We define SIR_{ave} as the ratio of average signal power to the average interference power. Our goal is to calculate SIR_{ave} when ICI is mitigated and compare it to that of the "no mitigation" case. Consider a narrowband time-variant channel, $h^{(i)}$. Note that we drop the index k of $h_k^{(i)}$ in this section under narrowband channel assumption. Then, in the absence of noise, (3) can be simplified as follows:

$$y_i = h^{(i)} \times x_i \qquad (28)$$

The estimate of x_i will be

$$\hat{x}_i = \frac{y_i}{\hat{h}^{(i)}} = x_i + \frac{e_i}{\hat{h}^{(i)}} \times x_i \qquad (29)$$

In (29), $e_i = h^{(i)} - \hat{h}^{(i)}$. Since $\hat{h}^{(i)}$ is the sum of a considerable number of uncorrelated random variables as estimated from pilot tones, we approximate its distribution with a complex Gaussian. In practice if $\hat{h}^{(i)}$ is having near to zero values, the received signal will not be divided by it. From theoretical standpoint, if the cases of near to zero $\hat{h}^{(i)}$ are not excluded, the variance of $\hat{x}_i$, the estimate of x_i, will be infinite (this can be seen from the results of this section). Therefore, we need to exclude the probability of a near to zero $\hat{h}^{(i)}$ to make the analysis meaningful. This can be done by introducing a slight modification in the pdf of $|\hat{h}^{(i)}|^2$. Let $prob(|\hat{h}^{(i)}|^2 \leq \mu) = \epsilon$. Then, for an ϵ near zero, we take the pdf of $|\hat{h}^{(i)}|^2$ to be zero for $|\hat{h}^{(i)}|^2 \leq \mu$.

Taking an FFT of (29), we will have

$$\hat{X}_i = X_i + A_i \qquad (30)$$

In (30), $a_i = \frac{e_i}{h^{(i)}} \times x_i$ and A_i is the FFT of it. A_i is not purely interference and contains a term that depends on X_i as well. However, it can be shown that the power of that term is considerably small. Therefore, to reduce the complexity of the analysis we take A_i as the interference term which makes the analysis a tight approximation. SIR_{ave} can then be defined as follows:

$$SIR_{\text{ave}} = \frac{\sigma_X^2}{\sigma_A^2} \qquad (31)$$

where σ_X^2 is the average power of X and σ_A^2 can be calculated as follows:

$$\sigma_A^2 = E(A_i A_i^*) = \sum_{n=0}^{N-1} \sum_{m=0}^{N-1} E(a_n a_m^*) e^{-\frac{j2\pi i(n-m)}{N}}. \qquad (32)$$

Since $E(x_n x_m^*) = (\sigma_X^2/N)\delta_{n,m}$, then

$$\sigma_A^2 = \frac{\sigma_X^2}{N} \times \sum_{m=0}^{N-1} E\left(\left| \frac{e_m}{\hat{h}^{(m)}} \right|^2 \right) \qquad (33)$$

and we will have

$$SIR_{\text{ave}} = \frac{N}{\sum_{m=0}^{N-1} E\left(\frac{|e_m|^2}{|\hat{h}^{(m)}|^2} \right)}. \qquad (34)$$

Both e_m and $\hat{h}^{(m)}$ have complex Gaussian distributions. Furthermore, they are jointly Gaussian (since a linear combination of them is the sum of a considerable number of uncorrelated random variables) and correlated. Then, $E\left(\left| \frac{e_m}{\hat{h}^{(m)}} \right|^2 \right)$ will be as follows (derived in Appendix D):

$$E\left(\left| \frac{e_m}{\hat{h}^{(m)}} \right|^2 \right) = \frac{\rho_m^2 \sigma_{e_m}^2}{\sigma_{\hat{h}^{(m)}}^2} + \sigma_{e_m^2}\left(1 - \rho_m^2\right) E\left(\frac{1}{|\hat{h}^{(m)}|^2} \right). \qquad (35)$$

In (35), $\sigma_{\hat{h}^{(m)}}^2 = E(|\hat{h}^{(m)}|^2)$, $\sigma_{e_m}^2 = E(|e_m|^2)$ and $\rho_m = E(e_m \hat{h}^{(m)*})/\sigma_{e_m}\sigma_{\hat{h}^{(m)}}$. These parameters are functions of channel correlation characteristics (or Doppler spectrum) and are derived in Appendix D. Also, it can be easily shown that $E(1/|\hat{h}^{(m)}|^2) = Ei(-ln(1 - \epsilon))/\sigma_{\hat{h}^{(m)}}^2$ where Ei and ln stand for the exponential integral and logarithm in the base of e respectively. Inserting (35) in (33) will result in the following SIR_{ave}:

$$SIR_{\text{ave}} = \frac{N}{\sum_{m=0}^{N-1} \frac{\sigma_{e_m}^2 \times \rho_m^2 + Ei(-ln(1-\epsilon)) \times (1-\rho_m^2) \times \sigma_{e_m}^2}{\sigma_{\hat{h}^{(m)}}^2}}. \qquad (36)$$

Fig. 4 shows SIR_{ave} of (36) as a function of $f_{d,\text{norm}}$ at $\epsilon = 10^{-6}$. $f_{d,\text{norm}}$ is defined as f_d (maximum Doppler) divided by the sub-carrier spacing. Channel power spectrum is Jakes spectrum [19] for this result. This means that function R of Appendix D is $R(t) = J_0(2\pi f_d t)$ with J_0 representing

DOCKET ALARM

Explore Litigation Insights

Docket Alarm provides insights to develop a more informed litigation strategy and the peace of mind of knowing you're on top of things.

Real-Time Litigation Alerts

Keep your litigation team up-to-date with **real-time alerts** and advanced team management tools built for the enterprise, all while greatly reducing PACER spend.

Our comprehensive service means we can handle Federal, State, and Administrative courts across the country.

Advanced Docket Research

With over 230 million records, Docket Alarm's cloud-native docket research platform finds what other services can't. Coverage includes Federal, State, plus PTAB, TTAB, ITC and NLRB decisions, all in one place.

Identify arguments that have been successful in the past with full text, pinpoint searching. Link to case law cited within any court document via Fastcase.

Analytics At Your Fingertips

Learn what happened the last time a particular judge, opposing counsel or company faced cases similar to yours.

Advanced out-of-the-box PTAB and TTAB analytics are always at your fingertips.

API

Docket Alarm offers a powerful API (application programming interface) to developers that want to integrate case filings into their apps.

LAW FIRMS

Build custom dashboards for your attorneys and clients with live data direct from the court.

Automate many repetitive legal tasks like conflict checks, document management, and marketing.

FINANCIAL INSTITUTIONS

Litigation and bankruptcy checks for companies and debtors.

E-DISCOVERY AND LEGAL VENDORS

Sync your system to PACER to automate legal marketing.

fastcase®
Smarter legal research.